

# Milestone 2 Final Report: Shaped Pupil Narrowband Contrast

Eric Cady<sup>1</sup>, Xin An<sup>1</sup>, Bala Balasubramanian<sup>1</sup>, Rosemary Diaz<sup>1</sup>, N. Jeremy Kasdin<sup>2</sup>,  
Brian Kern<sup>1</sup>, Andreas Kuhnert<sup>1</sup>, Bijan Nemati<sup>1</sup>, Keith Patterson<sup>1</sup>, Ilya Poberezhskiy<sup>1</sup>,  
A. J. Riggs<sup>2</sup>, Daniel Ryan<sup>1</sup>, Hanying Zhou<sup>1</sup>, Robert Zimmer<sup>1</sup>, Neil Zimmerman<sup>2</sup>

January 14, 2015

## 1 Overview

As laid out in original definitions to NASA Headquarters and the Technology Assessment Commitment (TAC), AFTA-C Milestone 2 was defined as:

*The shaped pupil coronagraph in the High Contrast Imaging Testbed demonstrates  $10^{-8}$  raw contrast with narrowband light at 550 nm in a static environment.*

In this report, we will present repeated convergence to a  $\sim 6 \times 10^{-9}$  mean contrast in the High Contrast Imaging Testbed (HCIT), across a  $4.4\text{--}11.2\lambda/D$  wedge-shaped dark hole with a shaped-pupil characterization mask in a 2% band centered around 550nm. These materials were due September 30, 2014 to the TAC; milestone materials were presented to the TAC September 17th and reviewed with the TAC October 8th.

Section 2 will lay out the technical background behind the development of the shaped pupil coronagraph and its mask designs, and Section 3 will detail the hardware and software used for the testing. These results and their associated analysis, including estimates of planet yield given the results seen in the testbed, are presented in Section 4.

## 2 Technical background

The concept of the shaped pupil coronagraph (SPC) is based in the principles of Fourier optics: under certain assumptions (e.g. paraxial beam), the relationship between the electric fields at a pupil plane and at a focal plane in an optical system can be well represented by a Fourier transform. Given a circular aperture, for example, the wavefront from a point source will be focused into an amplitude distribution  $\propto J_1(x)/x$ , giving rise to the well-known Airy pattern in its point spread function (PSF). With a shaped pupil, that circular aperture is replaced by a shape—generally chosen by an optimization process—whose Fourier transform has regions where the amplitude of the fields is extremely low, producing a high contrast between the peak of the PSF and these regions in the wings. Should a planet be present off-axis, it will be detectable in these regions. (Figure 1 gives an example of this relationship.)

At its simplest, a shaped stop in a pupil plane is the entirety of the coronagraphic optics in the SPC, barring the addition of a field stop to keep the camera from saturating from the high dynamic range involved. This makes the shaped pupil both straightforward to implement and quite robust to low order errors, as they have to be quite large to induce significant effects on the shape of the PSF. However, the converse of

---

<sup>1</sup>Jet Propulsion Laboratory, California Institute of Technology, Pasadena, CA, 91109 USA

<sup>2</sup>Dept. of Mechanical and Aerospace Engineering, Princeton University, Princeton, NJ, 08544 USA

©2015 California Institute of Technology. Government sponsorship acknowledged.

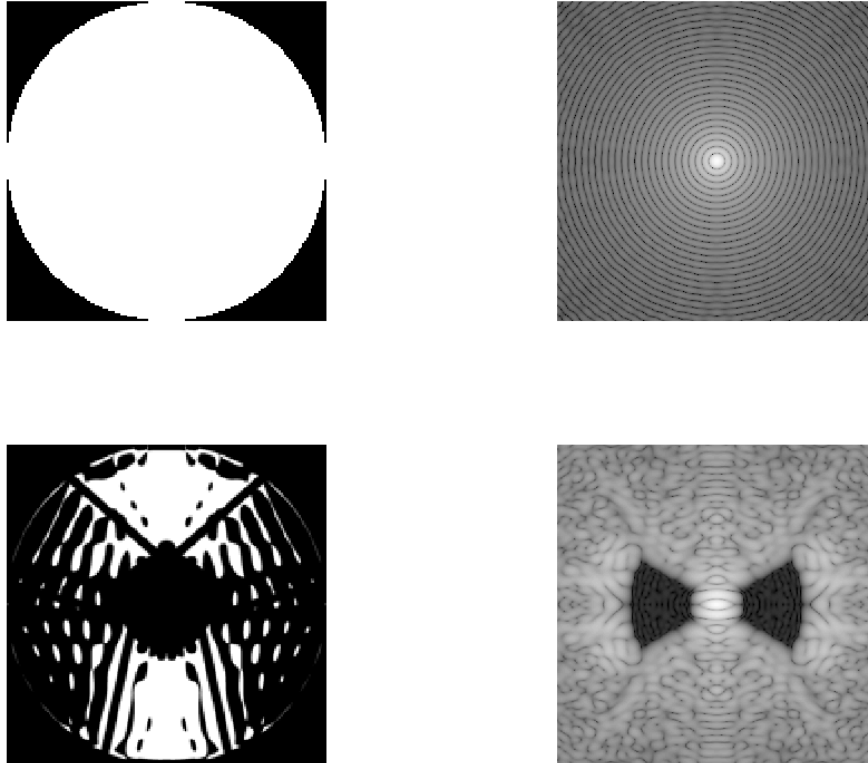


Figure 1: *Top:* In its focal plane, an unobstructed circular aperture produces an Airy pattern: a circularly-symmetric point spread function whose falloff with radius is too slow to permit the detection of nearby planets. *Bottom:* In its focal plane, a shaped pupil creates regions of high contrast where planets may be observed.

this simplicity is reduced science yield: other concepts, such as the hybrid Lyot coronagraph (HLC), are expected to have the capability to have deeper contrasts and work closer to the star.

The shaped pupil Lyot coronagraph (SPLC) was created to try improve science capability without sacrificing too much of the robustness of the shaped pupil; it will use the field stop actively as a focal plane mask and augment this with a Lyot stop at a downstream pupil. This development was not finished by Milestone 2, but an SPLC is expected to be tested out as a part of the next shaped pupil contrast milestone (AFTA-C Milestone 5).

Two general classes of mask are being optimized for AFTA-C: characterization and disk science. Characterization masks use sets of wedged dark regions to improve their inner working angle (IWA), but require multiple exposures to image the whole of the area around the star. To compensate for this on AFTA-C, they are expected to be used with the integral field spectrograph (IFS) to spectrally characterize planets whose focal-plane locations have already been determined. Disk science masks have poorer inner working angle, but can create a dark region  $360^\circ$  about the star for imaging of disk structures. For Milestone 2, a characterization mask was used with a dark hole running from  $4.4 - 11.2\lambda/D$  in a  $52^\circ$  wedge.

Shaped pupils in the past have been transmissive, primarily using holes etched through wafers with deep reactive ion etching (DRIE) to create the pupil shape. These masks were freestanding and self-supporting, and were successfully demonstrated at high contrast in the HCIT previously, including  $4 \times 10^{-9}$  contrast in monochromatic, 790nm laser light with 2DMs in the summer of 2013 [1]. Unfortunately, the features of the AFTA pupil—secondary, spiders, and additional small circles around the secondary—proved hostile enough to optimization that pupil shapes could not be found without small isolated regions that could not be built in a freestanding optic, and new technology was required. This was not the case for the field stops, and they have continued to be produced as etched apertures in wafers.

A few transmissive masks had been created on a transparent substrate for specific applications, but the ghosts induced by internal reflections off the substrate surfaces have not made these designs suitable for contrasts at the levels required by AFTA. Instead, the mask was made reflective, with nominally-open region coated with reflective metal and the dark region created from a highly-absorbing material: black silicon. (Subsequent technology development has shown that substrates exist with sufficiently-low reflectivity that transmissive masks could be potentially be manufactured for very-high-contrast applications, but they have yet to be qualified to the level of reflective designs.)

## 3 Facility and experiment design

### 3.1 Masks

The milestone 2 mask is a  $35\text{mm} \times 35\text{mm}$  diced section of a silicon wafer 2mm thick. This mask is coated with bare aluminum, and black silicon is used to create the dark regions of the pupil. An image of the mask is shown in Figure 2. Milestone 1 previously demonstrated that this mask, as manufactured, was sufficient to permit demonstrations at the contrast level required for Milestone 2. The mask thickness was selected to help minimize wafer bow, which introduces undesirable low-order phase aberrations into the pupil; in addition, a pre-selection process was done to find wafers with minimal Zernike components above focus in the prospective shaped-pupil region. Focus can be compensated for at a system level by translating the camera and field stop; this proves fortunate, as the focus component of the Milestone 2 mask introduces microns of wavefront, well outside the stroke capability of our DM.

An array of field stops were etched into a  $24\text{mm} \times 16\text{mm}$  section of an SOI wafer. Figure 3 shows the detail of one stop taken in transmission with a microscope as part of manufacturing validation. (The form of the field stops sized for shaped pupils with wedge-shaped regions of high suppression, such as in Figure 1, has led them to be termed generally as “bowtie masks”.) The angular sizes of the bowties were undersized with respect to dark-hole wedge angle, which was  $60^\circ$ ; upcoming SPLC designs use  $70^\circ$  wedges on their dark holes so even an undersized focal plane mask permits wedges greater than  $60^\circ$ .



Figure 2: A downsampled version of high-resolution microscope imagery of the Milestone 2 mask, taken as part of manufacturing validation. The background lines are a stitching artifact.

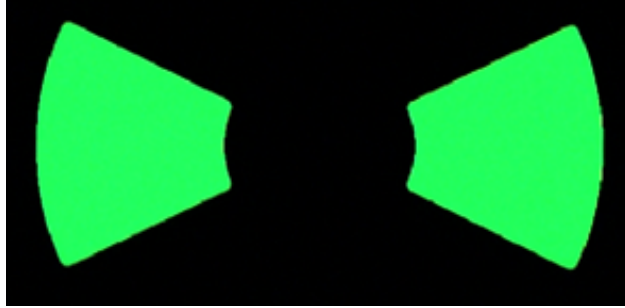


Figure 3: A high-resolution image, in transmission, of a single bowtie mask. Distance from the left edge to the right edge is approximately  $430\mu\text{m}$ .

### 3.2 Optical layout and hardware

Figure 4 shows the optical layout of the HCIT as designed. In addition to the basic requirements of the shaped pupil architecture (reflective shaped pupil, bowtie mask for dynamic range, at least 1 DM), two other considerations drove the final layout:

- **Prompt execution:** The shaped pupil contrast milestone was the first testbed-demonstration milestone for the AFTA coronagraph. In order to get the testbed ready early to meet this milestone, the layout was designed to reuse existing optics as much as possible, including recycling all of the off-axis parabolas currently in use on the HCIT bench, and so avoiding lengthy procurements. This decision also fixed the focal lengths in the system, necessitating additional folds to keep it confined to the optical table.
- **Future expansion:** While the initial layout only included a single DM and a reflective shaped pupil, it was designed to be compatible with the full extent of the OMC architecture. Surrogate folds were added so that a second DM and a fast steering mirror could be swapped into those locations later, and a focal plane prior to the shaped pupil was kept free so a HLC could be used there, along with a reflective Lyot stop. Despite the eventual plan to use two DMs, only one was available when the testbed was first assembled. The shaped pupil does not require 2 DMs to create high contrast in a half-plane region, and given the uncertainties in the schedule of this procurement process, Milestone 2 was not specified to require 2DM control for completion.

### 3.3 Software and algorithms

Wavefront estimation is done with a pairwise estimation scheme, in which “probes” are placed on the DM to modulate the electric field across the region of interest. For our purposes, these probes are made from a combination of sinc and sine functions chosen such that the probe amplitude over the region of interest is relatively uniform. Given two or more pairs of probes, along with a images with no probes at all, we can back out both the complex electric field of the residual simulated starlight and the portion of the field that does not interact with the probes and hence is unlikely to be correctable. (The components that do and do not interact with the probes are referred to as the “coherent” and “incoherent” parts, respectively.) For further detail of the algorithm, see [2].

Wavefront correction is done with an algorithm called electric field conjugation (EFC), which chooses DM settings to minimize the electric field across the dark hole, using a model of the coronagraph and DM. A regularization parameter is included to weigh the relative importance of the data versus the model, and this parameter is tuned by taking a series of extra images per iteration. For more detail on EFC, see [3].

Testbed control during experiments was performed using existing HCIT software for remote control of actuators, DMs, light sources, and the camera. This software implements two loops which run concurrently:

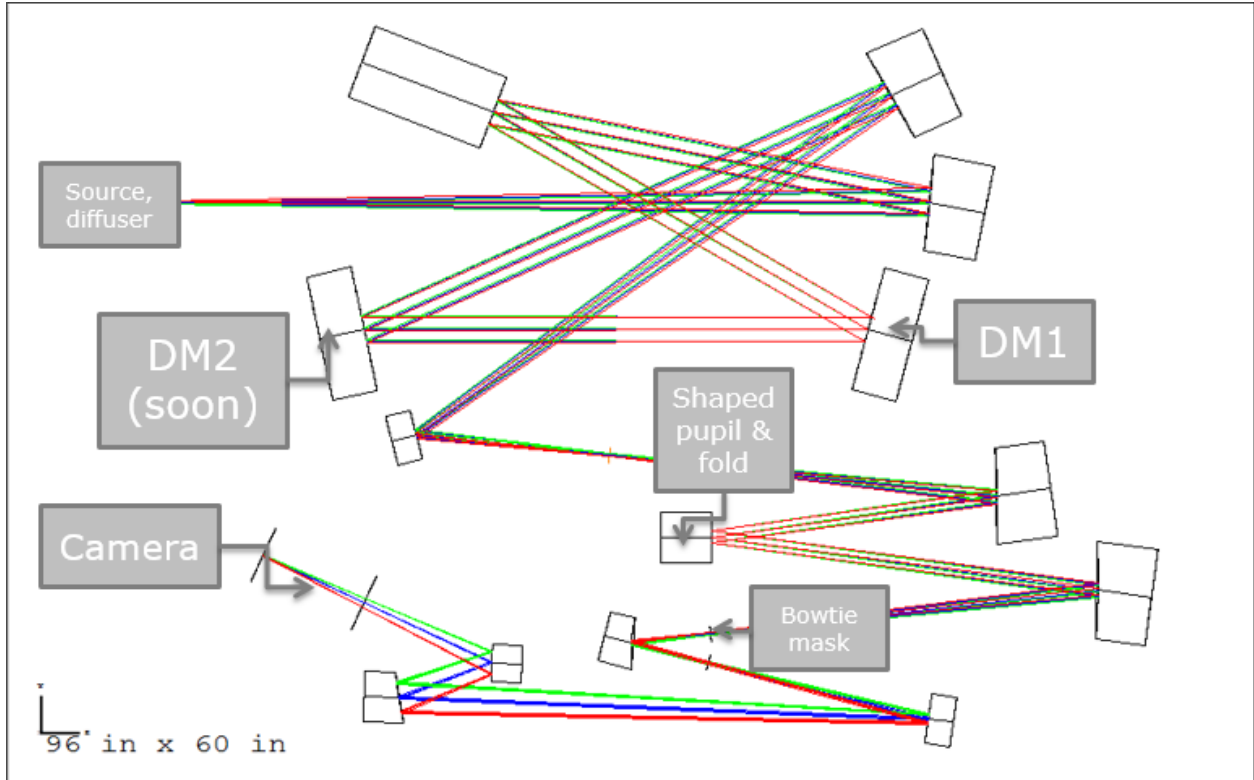


Figure 4: A Zemax layout of the testbed in tank HCIT-1 during the Milestone 2 tests. The text overlay points out salient hardware. The camera is mounted on a 10-inch stage, permitting it to reach both the pupil and focal planes indicated by black lines crossing the ray trace. As of the writing of this report, DM2 has been installed.

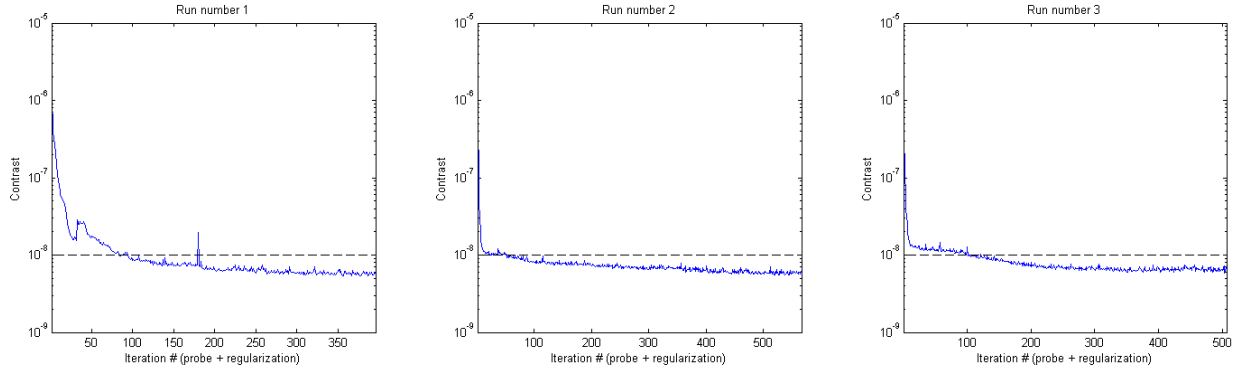


Figure 5: Mean contrast across the dark hole as a function of iteration number, for each of the three Milestone 2 runs. Run 1 contained manual interventions while testing appropriate parameters for the run, producing the plateau near iterations 30-50 and around iteration 180.

Table 1: Contrast data for 3 Milestone 2 runs

Run	#1 (8/28-8/29)	#2 (8/29-8/30)	#3 (8/30-8/31)
Contrast over final 100 iterations	$(5.85 \pm 0.49) \times 10^{-9}$	$(5.95 \pm 0.49) \times 10^{-9}$	$(6.59 \pm 0.56) \times 10^{-9}$
99% CI on mean contrast in dark hole	$[5.54 \times 10^{-9}, 6.16 \times 10^{-9}]$	$[5.64 \times 10^{-9}, 6.26 \times 10^{-9}]$	$[6.23 \times 10^{-9}, 6.94 \times 10^{-9}]$

one interfaces at a low-level with the testbed hardware, putting probes on the DM and taking images, while the other does the high-level wavefront estimation and correction. Interfaces between the loops are handled by passing of data files containing either desired DM commands or photometrically-corrected camera images.

## 4 Data and analysis

For the milestone demonstration, we collected three independent sets of data between 8/28/2014 and 8/31/2014, each attempting to minimize the residual light across the dark hole, which was chosen to match the size of the bowtie:  $4.4 - 11.2\lambda/D$ . For consistency, each run started from a flat-DM setting obtained earlier during testbed calibration. (Using three independent runs starting from flat has been a standard method of demonstrating coronagraph capability during previous demonstrations under the TDEM program, and the practice was continued for the AFTA-C milestones, although starting from a previously-good DM setting produces much faster convergence.) Each run was allowed to continue until the contrast level had ceased to change; Figure 5 shows the progression of contrast over time. In each case, the contrast variation over the final 100 iterations was small, and Table 1 gives both 1) the estimate for the mean contrast across the dark hole over the final 100 iterations, and 2) a 99% confidence interval on the mean contrast achieved in the dark hole. Both show that the contrast level is significantly below the milestone threshold contrast of  $1 \times 10^{-8}$ , and is repeatable from run to run.

The contrast is not uniformly distributed over the dark hole: the upper right and lower left corners of the dark hole are particularly bright, with large incoherent components, and these drive the estimates of contrast as a function of radius. See Figures 6 for the contrast distribution across the dark hole and its incoherent parts, and Figure 7 for curves of contrast versus radius for the three runs.

While planet-yield estimation may currently be somewhat fuzzy—relying on assumptions on post-processing that are primarily hypothesized—we can make some estimates to ensure that the contrasts we are demonstrating in the laboratory have some traceability to expected science with AFTA-C. Working on the AFTA-C assumptions of  $10\times$  post-processing, we expect 10 known-radial-velocity planets to be detectable with SNR of 5, assuming a 2% band (i.e. looking through the IFS). If  $30\times$  postprocessing is possible, we expect that number to rise to 14. (Planet locations and radial contrast averages are shown in Figure 8.) The

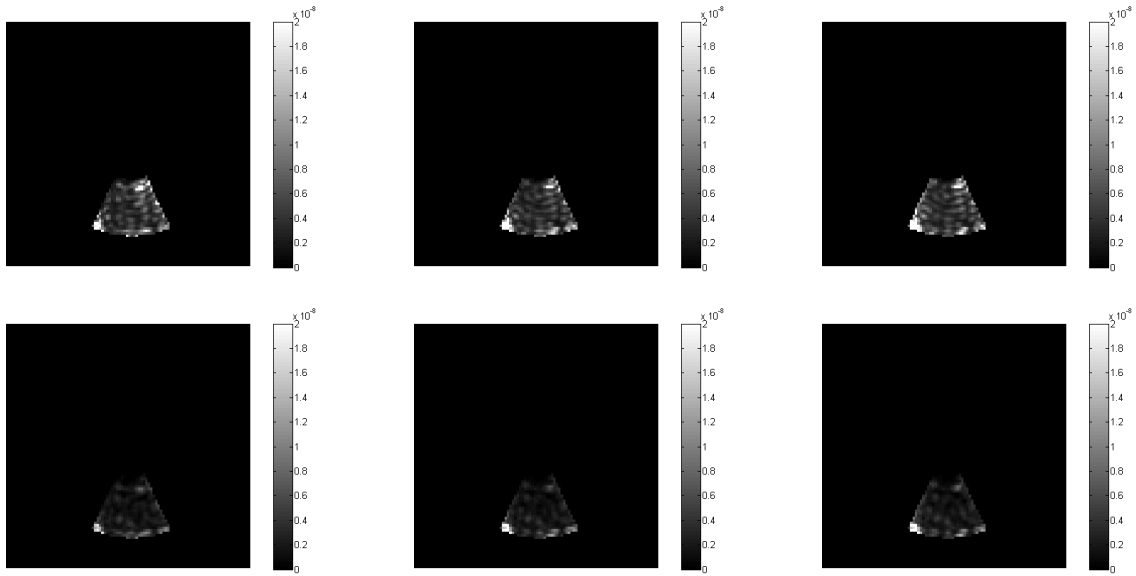


Figure 6: *Top*: Average light distribution across the dark hole for each of the three runs. Area outside the dark hole is masked in software. *Bottom*: The incoherent part (the portion of the intensity that cannot be modulated by the probes) for each of the three runs. The color scale in all images is identical and linear from 0 to  $2 \times 10^{-8}$ .

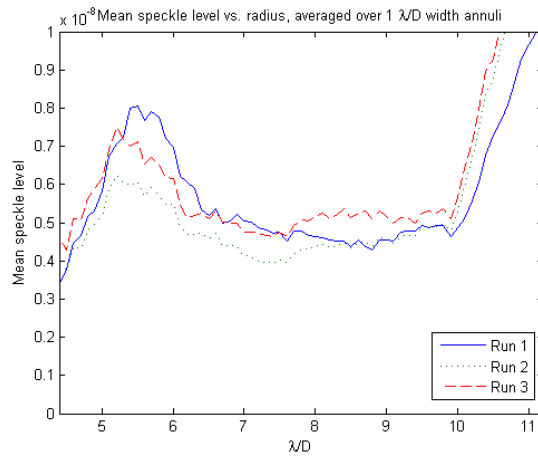


Figure 7: Average radial contrast distribution for the three runs. At each radial position, contrast is averaged over a  $1\lambda/D$  annulus centered at that radius.

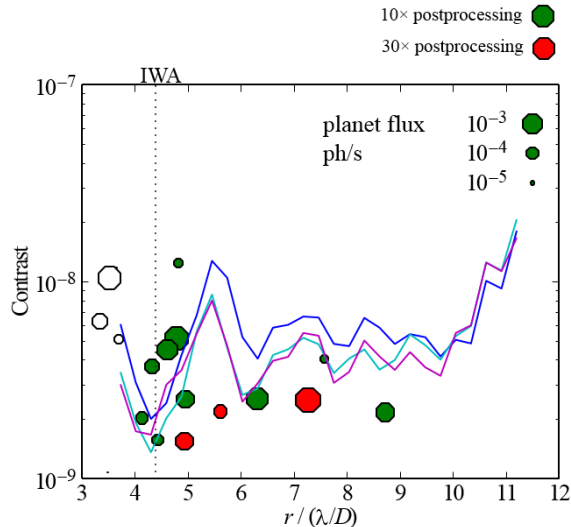


Figure 8: Distribution of known radial velocity planets with contrast curves from the three runs. Planet size shows the expected flux at the IFS detector in a 2% band. Green planets are detectable with 10 $\times$  post-processing at SNR = 5; red planets are not detectable without 30 $\times$  post-processing. One red planet falls below the x-axis of the plot and is not visible.

next-generation SPLC is expected to have a higher yield than this, particularly thanks to its smaller IWA.

For lagniappe, while Milestone 2 requirements made no mention of broadband performance, we took advantage of the flexibility of the VARIA to do a 2% correction at 550nm and examine performance with a 10% band also centered at 550nm. For this, we started correcting from the end point of run 2 to minimize number of iterations, and indeed it only took 2 iterations to bring the mean contrast in the dark hole back to  $\sim 6 \times 10^{-9}$  even after the passage of several days. Despite not correcting the ends of the band explicitly, the contrast remained quite low:  $9.1 \times 10^{-9}$  mean across the dark hole. (An image of the data, photometrically corrected, is shown in Figure 9.) This is consistent with the definition of Milestone 5, which is to show better than  $10^{-8}$  contrast in a 10% band.

## 5 Summary and next steps

We have demonstrated here that the shaped pupil coronagraph is capable of repeatedly reaching contrasts suitable for imaging planets with AFTA-C, with  $\sim 6 \times 10^{-9}$  contrast averaged across the dark hole. We have strong indications we will be able to continue to reach good contrasts in subsequent broadband tests for later milestones, and we have new designs expected to push this performance to better inner working angles and higher throughputs.

Our next immediate priorities are to prepare for, and execute, the Milestone 5 tests. To this end, a second DM has already been installed, although the electronic noise on the first has not been fully resolved. (Should tracing that prove fruitless, we will replace it with a 32x32 DM running on a different set of electronics and continue.) Additional testing we have planned includes estimation in low-flux conditions; open-loop testing of sensitivity to tip, tilt, and focus on the input beam; and validation of such error budget terms as can be tested with existing hardware and actuation. In the summer of 2015, the dynamic OMC testbed will be commissioned, where coronagraph performance validation will continue with perturbed input wavefront and low-order wavefront sensing and control subsystem working toward demonstrating Milestone 9 on 9/30/2016.

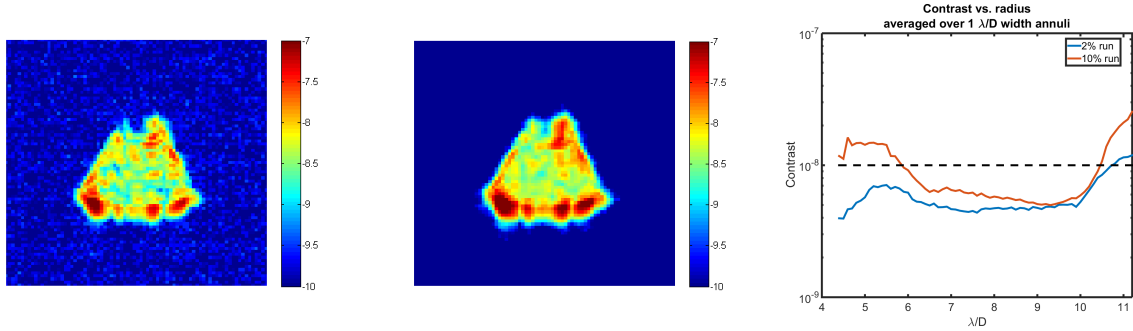


Figure 9: *Left:* Dark hole in 2% band centered at 550nm. *Center:* Dark hole in 10% band centered at 550nm, taken with same DM setting. Note that both are scaled to show the same contrast level; as the rightmost image is  $5\times$  as bright, the dark noise is pushed below the threshold of the color scale and the dark noise is not visible. *Right:* Radially-averaged contrasts for the left and right images.

## Acknowledgment

The research was carried out at the Jet Propulsion Laboratory, California Institute of Technology, under a contract with the National Aeronautics and Space Administration.

## References

- [1] A. J. E. Riggs, T. D. Groff, A. Carlotti, N. J. Kasdin, E. J. Cady, B. D. Kern, and A. Kuhnert. Demonstration of symmetric dark holes using two deformable mirrors at the high-contrast imaging testbed. In *Society of Photo-Optical Instrumentation Engineers (SPIE) Conference Series*, volume 8864 of *Society of Photo-Optical Instrumentation Engineers (SPIE) Conference Series*, page 0, September 2013.
- [2] A. Give'On, B. D. Kern, and S. Shaklan. Pair-wise, deformable mirror, image plane-based diversity electric field estimation for high contrast coronagraphy. In *Society of Photo-Optical Instrumentation Engineers (SPIE) Conference Series*, volume 8151 of *Society of Photo-Optical Instrumentation Engineers (SPIE) Conference Series*, September 2011.
- [3] Amir Give'on. A unified formalism for high contrast imaging correction algorithms. volume 7440, page 74400D. SPIE, 2009.